JOURNAL OF CATALYSIS 133, 55–82 (1992)

The Controlled Dispersion of Silica Supported MoO_3: The Role of Ammonia

ABHAY K. DATTA, JIN-WOOK HA, AND JOHN R. REGALBUTO[1]

Department of Chemical Engineering, University of Illinois at Chicago, 810 S. Clinton, Chicago, Illinois 60607

Received April 16, 1991; revised July 8, 1991

The morphology of silica supported catalysts, prepared by impregnation of ammonium heptamolybdate and for various weight loadings up to 35 wt%, was studied using X-ray diffraction, transmission electron microscopy, and X-ray photoelectron spectroscopy. In addition to the orthorhombic phase, the behavior of the rarely studied hexagonal phase was fully characterized. All morphologies of silica supported MoO_3 appear to be thermodynamically driven. At low loadings there appeared one stable dispersion, independent of initial precursor dispersion. For high loaded catalysts there appeared three states: a metastable sintered hexagonal state and a well dispersed hexagonal state at moderate temperature calcinations (300°C), and the sintered orthorhombic state at high temperature (500°C). Whereas the sintered orthorhombic phase is detected by XRD at loadings in excess of 1.1 atom Mo/nm^2, the well dispersed hexagonal phase is not evident until 4.0 atoms Mo/nm^2. It is possible to produce the well dispersed hexagonal phase from the sintered orthorhombic phase with an ammonia impregnation and subsequent calcination at 300°C. The apparently higher dispersion of the hexagonal phase may arise from some role of ammonia which results in a stronger MoO_3–surface interaction.

INTRODUCTION

Supported molybdenum trioxide catalysts have a vast abundance of industrial uses. Continual effort is put into characterization of the types of Mo oxide species which exist over various supports, their stability, and the optimal preparation techniques to obtain them. Various morphology influencing factors have been proposed for the impregnation and calcination steps of preparation. For example, a strong adsorption technique (*1*) has been employed to ensure that the negatively charged ionic complexes of molybdenum are uniformly adsorbed onto a positively charged surface (in an aqueous phase at a pH below the isoelectric point of the oxide). Many other groups have cited the importance of the oxide isoelectric point and other electrochemical factors regarding impregnation, a positive surface charge being necessary to achieve good dispersion of the negative Mo complexes adsorbed from liquid solution (*2–9*). On the other hand, a number of groups have reported that well dispersed morphologies can be produced simply by calcining mechanical mixtures of MoO_3 with the oxide supports (*10–17*), implying that morphology arises from a thermodynamic solid–solid wetting process. *In situ* Raman studies have shown that the degree of surface hydration strongly influences the Mo species present (*6, 18–23*). Allyl complexes (*24–27*) and chloride complexes (*17, 28–31*) which interact with surface hydroxyl groups have been used in an attempt to initiate and maintain good molybdenum dispersion. Other authors have cited correlations between the number of Mo species deposited and the number of "reactive" hydroxyl groups (*6, 7, 32*).

A recent series of comprehensive works performed with Raman and UV over a number of supports and supported oxides and with a wide array of preparation procedures,

[1] To whom correspondence should be addressed.

0021-9517/92 $3.00

including all those listed above, have synthesized many of these concepts into a general theory (*33–36*). First, it was postulated that the surface species of molybdenum present in the air exposed, hydrated catalyst is only a function of pH in the hydrated layer, which can be calculated from the point of zero charge (or "pzc," which is equivalent to the isoelectric point in the absence of specific adsorption) of the oxide, adjusted for the surface composition of molybdenum oxide or other oxide. The types of surface species are independent of the preparation procedure and complex. Second, the amount of material deposited in well dispersed form depends on the number of reactive hydroxyl groups present. For example, large amounts of well dispersed species can form over alumina and titania, which have high hydroxyl group surface densities, but only small amounts can form on silica, which has a low hydroxyl density (*33*). Presumably, over the same support, allyl and chloride complexes exhibit a higher dispersion because they interact with the support at low temperatures at which more hydroxyl groups are present, whereas with typical impregnations with ammonium salts this interaction occurs at a high calcination temperature at which the surface is substantially dehydroxylated. This general picture would appear to be a good yardstick with which to compare any new characterization results of supported metal oxide systems.

It is generally agreed that over alumina, molybdena exists at lowest loadings as a monomeric, tetrahedrally coordinated species, at higher loadings, as polymeric but well dispersed octahedrally coordinated species, and finally, at higher loadings as poorly dispersed bulk MoO_3 (*2, 18, 37–39*). Molybdenum can also form compounds with this strongly interacting support. According to the general theory above, at low loadings of molybdena the pzc of alumina isn't appreciably affected by MoO_3 surface groups, so the pH of the hydrated layer remains high and the resulting Mo species are monomeric (tetrahedral). At higher loadings, however, the pzc is brought down by acidic Mo species to the point where the pH in the hydrated layer is that at which the octahedral Mo complexes form (*35*). Alumina is often the choice of oxide support for molybdena, since the stronger interaction means that the well dispersed and more catalytically active forms of molybdena persist to higher loadings. A common value cited for maximum surface loading before the onset of bulk MoO_3 over alumina is about 5 atoms/nm^2 (*6, 36, 39, 40*).

There is still discussion as to the nature of surface species over silica. Many reports have it that the monomeric surface species exist at low loadings, polymeric at intermediate loadings, and bulk at high loadings, roughly in parallel to alumina, except that the formation of the polymolybdate and the bulk species occurs at lower loadings (*18, 24, 41–48*). More recent *in situ* works (*35, 49*), in which only the polymeric species is observed before the formation of the bulk form at higher loadings, have brought this idea into question. According to the general synthesis theory as pertains silica (*35*), the pzc of silica is very low and so low pH values of the hydrated layer are always present giving rise only to the polymeric, octahedral species. Tetragonal signals were shown to arise from $NaMoO_3$ and $CaMoO_4$ crystalline impurities stemming from Na and Ca impurities in precipitated silica.

Silica is a more weakly interacting support than alumina, as Mo–Si compounds do not form and the reported loadings at which bulk compounds form are much lower. Whereas a high temperature calcination of a mechanical mixture of MoO_3 with alumina, titania, zirconia, or magnesia will result in the extensive or complete redispersion of MoO_3, over silica it will not (*10, 13, 15, 16*). The maximum surface loading of molybdena before formation of bulk MoO_3 is much lower for silica than for alumina; given in Table 1 are values culled from the literature for weight loadings of the onset of bulk MoO_3. Values were taken from works in which series of samples with increasing

TABLE 1

Reported Onset of Bulk MoO_3 on SiO_2, AHM Impregnated Catalysts

Reference	Surface area (m^2/gm)	MoO_3 (Wt%)	Surface loading (atom Mo/nm^2)	Technique
(*28*)	397	12.0	1.3	XRD
(*41*)	633	17	1.1	XRD
(*44*)	179	8.2	1.9	XRD
(*45*)	384	13	1.4	XRD
(*47*)	450	5.0	0.48	XRD
(*48*)	40	2.4	2.4	XRD
(*49*)	465	10	0.90	XRD
(*51*)	360	8.6	1.0	XRD
(*52*)	672	9.0	0.56	XRD
(*53*)	240	8.6	1.5	TEM
(*51*)	360	3.4	0.4	TPR
(*45*)	384	5.0	0.54	XPS
(*18*)	782	5.0	0.27	Raman
(*35*)	280	0.4	0.09	Raman
(*44*)	179	6.7	1.6	Raman
(*47*)	450	2.0	0.19	Raman
(*48*)	40	1.2	1.2[a]	Raman
(*49*)	465	5.0	0.45[a]	Raman
Based on monomer area, 19 Å:			5.0	

[a] No lower loading tested.

loadings were studied; crystalline limits so derived are only approximate as only discrete weight loadings are reported. These are converted to atomic surface loading (atom Mo/nm^2) for the sake of comparison.

From Table 1 it is seen that the reported values of maximum loading before bulk formation are dependent on the characterization technique. Not surprisingly, a less sensitive technique, X-ray diffraction, yields the higher values. These average 1.1 atom/nm^2. The range of values is rather large; discrepancies may arise in part from the wide variety of X-ray diffractometers employed, but probably also indicate the differences in details of the impregnation techniques employed. With Raman spectroscopy, probably the most sensitive technique, values are much lower and average about 0.25 atoms Mo/nm^2. Of note is that whenever XRD was compared directly to a more sensitive characterization technique by the same research group (*44, 45, 47–49, 51*), the limit of crystallinity was observed to be lower than that established by XRD. This implies that a significant portion of MoO_3 can exist as microcrystalline material (*44, 45, 47, 48*), below the approximately 40 Å XRD limit of detection.

Molybdena surface loadings obtained from equilibrium adsorption preparations at low pH result in low surface loadings in the neighborhood of the Raman measurements; values of 0.38 (*1*) and 0.25 (*50*) atoms Mo/nm^2 have been reported. The maximum loading of well dispersed MoO_3 on silica is many times lower than that on alumina, by a factor as little as 5 or perhaps even as high as 50.

The present work with silica supported MoO_3 has centered on investigating and exploiting the behavior of the little studied hexagonal phase of MoO_3. In all of the above referenced work, molybdenum trioxide is produced by a calcination at temperatures in excess of 450°C, which produces the well known and characterized orthorhombic

MoO_3 phase. The hexagonal phase can be produced in unsupported or supported form by adding concentrated acid to an AHM solution and drying at room temperature; it is stable to approximately 420°C in air (*54–56*). The hexagonal phase is actually yet a precursor to the orthorhombic phase, for it possesses small amounts of ammonium ions and varying degrees of water as interstitial impurities, depending on preparation and drying conditions (*54*). The parent compound of various partially dehydrated and deammoniated phases is thought to be ammonium decamolybdate, $(NH_4)Mo_5O_{18}H_5$ (*54*), which can be written as $((NH_4)_2O) \cdot 10MoO_3 \cdot 5(H_2O)$ or $((NH_4)_2O)_{0.1} \cdot MoO_3 \cdot (H_2O)_{0.5}$ to emphasize the stability of the hexagonal MoO_3 framework. The hexagonal phase is observed on silica, with no acid, when the impregnated ammonium molybdate precursor is calcined at a temperature of 300°C, but in the absence of the silica support the bulk orthorhombic phase is formed instead (*55*), and without the ammonia containing precursor the orthorhombic form is produced by a 300°C calcination over silica (*55*). The unsupported forms are cited to convert irreversibly to the orthorhombic form upon a higher temperature calcination (*54–56*). Thus the hexagonal form is somewhat elusive, and there may not appear to be much motivation for its study.

In preliminary X-ray diffraction studies and in controlled atmosphere electron microscopy studies (*57*) of the molybdena/silica system, however, very interesting and potentially advantageous behavior of the hexagonal phase was observed. Whereas the formation of the orthorhombic phase at a high calcination temperature was accompanied by sintering and crystallite growth, at a lower temperature the formation of the hexagonal phase from large aggregates of the ammonium molybdate precursor was followed by continued disintegration of the crystallites, producing a highly dispersed form of MoO_3 at relatively very high surface loadings.

Better catalysts might result were higher loadings of well dispersed MoO_3 possible over silica, as the well dispersed forms have been shown to exhibit catalytic activity in the sulfided state as good as or better than the similar morphology over alumina (*36, 51*). Unsupported and large, supported hexagonal forms have exhibited higher activity for methanol oxidation than the respective orthorhombic forms (*58*).

It was in the interest of exploring further the redispersion behavior of the silica supported hexagonal MoO_3 phase and exploiting this behavior for the control of dispersion and the production of more highly dispersed MoO_3/SiO_2 catalysts that this work was undertaken. It appears that under certain conditions the hexagonal phase can be spread on SiO_2 to an extent much higher than that of the orthorhombic phase. It has been found that the genesis of a very well dispersed morphology does not depend directly on the production of the hexagonal phase at 300°C, but may be the somewhat coincidental effect of ammonia as a silica wetting agent. All morphologies produced are thermodynamically stable or metastable. An equilibrium phase model of all phases as a function of pretreatment conditions is derived. In this manner, the ability to control the morphology of silica supported MoO_3, even to the point of redispersing the sintered orthorhombic phase, is obtained.

EXPERIMENTAL

For high surface area catalysts, Degussa Aerosil (fumed) silica was used. The powder was 99.8% pure with traces of Al_2O_3, Fe_2O_3, TiO_2, and HCl. Na and Ca impurities in fumed silica are typically on the order of 2 ppm. The silica had a surface area of 380 ± 30 m^2/gm. To increase its bulk density, it was washed with deionized water and vacuum dried overnight at 40°C and then air dried at 110°C for 12 hr. Ammonium heptamolybdate (IV) tetrahydrate $(NH_4)_6Mo_7O_{24} \cdot 4H_2O$, (AHM), was purchased from Aldrich. High loading samples were prepared by physically mixing the desired amount of dry support and precursor, and then adding sufficient water to reach incipient wetness. This technique circumvents the problem at high loadings that the amount

of water added to the SiO_2 is insufficient to dissolve all of the AHM. This is typically resolved by performing successive impregnations with a lower concentration solution, whereas a single step was employed here. Acid or base impregnations were conducted with concentrated nitric acid (2.5 *N*) or ammonium hydroxide (5 *N*) in place of water. The acid preparation follows a standard procedure to produce hexagonal MoO_3 (*61–63*). MoO_3 weight loadings varied through 35.3% MoO_3. The most common weight loading studied, 26.7%, corresponds to a surface loading of 4 Mo atoms/nm^2. The slurries were thoroughly stirred and dried in air overnight, after they had been spread in a thin layer onto a watch glass. When samples were placed in a small crucible at depths of 1–2 cm, the top 2–3 mm of the sample turned darker (green) than the bulk of the sample after drying and calcination. Presumably some of the Mo containing phase migrated toward the surface during pretreatment. The final distribution of material appeared homogeneous with the use of watchglasses.

The resulting precursors from the "mix and wet" procedure were rather poorly dispersed, such that their X-ray diffraction patterns could be readily detected. (In contrast, no precursor XRD patterns were observed when a traditional impregnation with AHM dissolved in water was employed (*49*). Some samples were additionally dried at 110°C; this step was demonstrated to have no effect. Calcinations were performed in air in a standard muffle furnace. Unless otherwise specified, calcination times were 2 h.

Other samples were made by physically mixing hexagonal or orthorhombic MoO_3 and silica to the desired weight loadings, adding water to incipient wetness, and drying and calcining as before. This latter type of sample will be referred to as "physically mixed" and will be denoted "MoO_3 + SiO_2," whereas the former type will be referred to as "impregnated" and will be denoted "MoO_3/SiO_2."

X-ray diffraction was performed on one of two Siemens D 5000 diffractometers, at either 50 or 40 kV and 30 mA. For most samples (Figs. 1, 2, 3A, 5–8) approximately 50 mg of loosely packed powder was backfilled into a zero background holder. For Fig. 3B, 2 mg of sample was smeared onto a pyrex holder. For the same sample, the intensity of the backfilled patterns is approximately 30% higher than the smeared samples.

A similar preparation technique was used for low loading, high surface area samples used in conjunction with XPS measurements, except that to the physical mixtures of support and precursor an excess of liquid was added (wet impregnation) so that pH could be controlled and measured. These mixtures were dried in a rotary vacuum drier at 40°C and subsequently calcined in a muffle furnace. The spectroscopy was performed at the Amoco Research Center in Naperville, Illinois, using an SSX 100 spectrometer with an Al$K\alpha$ source at 25°C. All samples contained Mo in the +6 oxidation state. The Mo/Si ratio was used as an estimate of dispersion.

Model, low surface area catalysts for electron microscopy were prepared from planar silica substrates and nonporous silica spheres as described elsewhere (*57*). Briefly, dry impregnations as described above, with a surface loading of 4 atoms Mo/nm^2, were performed with the spherical silica powder. Samples were dispersed onto holey carbon substrates on gold finder grids. Catalyst impregnation was mimicked over the planar silica substrate by depositing a drop of the precursor solution onto the substrate and allowing the water to evaporate in air. Gold finder substrates were also used with the planar samples. A particular area of a sample was photographed through a series of calcination treatments. Microscopy was performed with a JEOL 100 CX, operated at 100 kV.

RESULTS

X-ray Diffraction Characterization of High Loading Catalysts

An X-ray diffraction study was first made of the unsupported and silica supported pre-

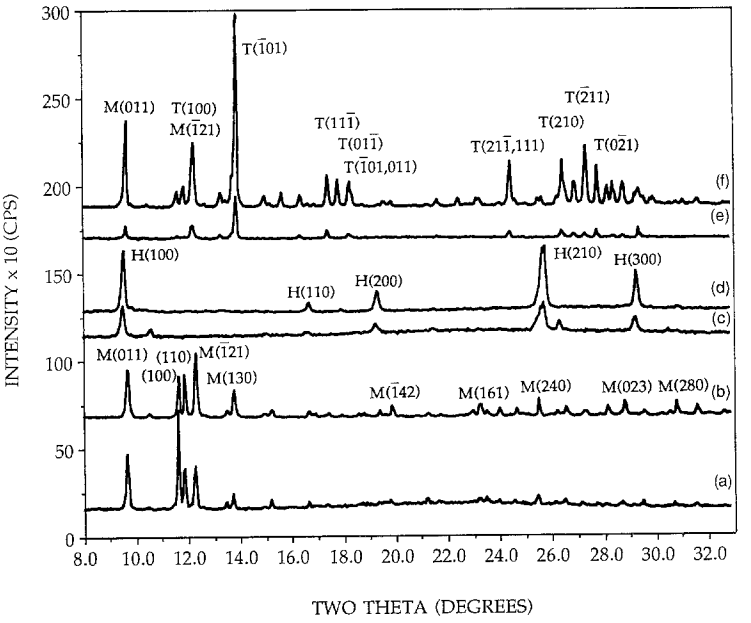

FIG. 1. XRD patterns of dried, unsupported and 36.5 wt% supported MoO_3: (a) supported, neutral AHM (monoclinic); (b) unsupported AHM; (c) supported acid precursor (hexagonal); (d) unsupported acid precursor; (e) supported basic precursor (mixed monoclinic and triclinic); (f) unsupported basic precursor.

cursor phases taken after drying at room temperature, as a function of pH of the liquid solution. The results are shown in Fig. 1. The monoclinic pattern of the water impregnated ammonium heptamolybdate (AHM) precursor, $(NH_4)_6Mo_7O_{24} \cdot 4H_2O$ is shown in pattern (b), and is unchanged from the stock material taken directly from the container. The precursor phase is also unchanged after AHM impregnation of silica at neutral pH, as seen in Pattern (a). Peaks for the silica supported samples in general are less intense due to dilution. With the addition of acid, both the unsupported (Pattern (d)) and supported (Pattern (c)) precursors are in the hexagonal form of MoO_3, or $((NH_4)_2O)_x \cdot MoO_3 \cdot (H_2O)_y$ ($0.05 \leq x \leq 0.1$, $y \leq 0.5$ (*54*)), at room temperature. With the addition of base (NH_4OH), some of the monoclinic $(NH_4)_6Mo_7O_{24} \cdot 4H_2O$ phase was still present, but a large fraction of it was converted to the triclinic phase $(NH_4)_2Mo_2O_7$ (*62*) (Pattern (f)). The same mixture of phases was seen for the supported sample, Pattern (e).

Thus the presence of silica appears to have no effect on the precursor phase found at any of the liquid pH values employed. This makes sense in light of the "mix and wet" impregnation procedure, in which the AHM was probably not completely dissolved in the liquid phase. However, the precursor form was a strong function of pH. The net effect of the acid was the lowering of the $NH_4^+ : MoO_3$ ratio in the solid phase, from 6 : 7 to 0.05 or 0.1 : 1, while the addition of base increased the $NH_4^+ : MoO_3$ ratio slightly to 1 : 1, according to

$$2(NH_4)_6Mo_7O_{24} + 2NH_3 + H_2O \rightarrow 7(NH_4)_2Mo_2O_7.$$

In terms of MoO_3 units, this can also be written as

$$14\,((NH_4)_2O)_{3/7} \cdot MoO_3 + 2NH_3 + H_2O \rightarrow 14\,((NH_4)_2O)_{1/2} \cdot MoO_3.$$

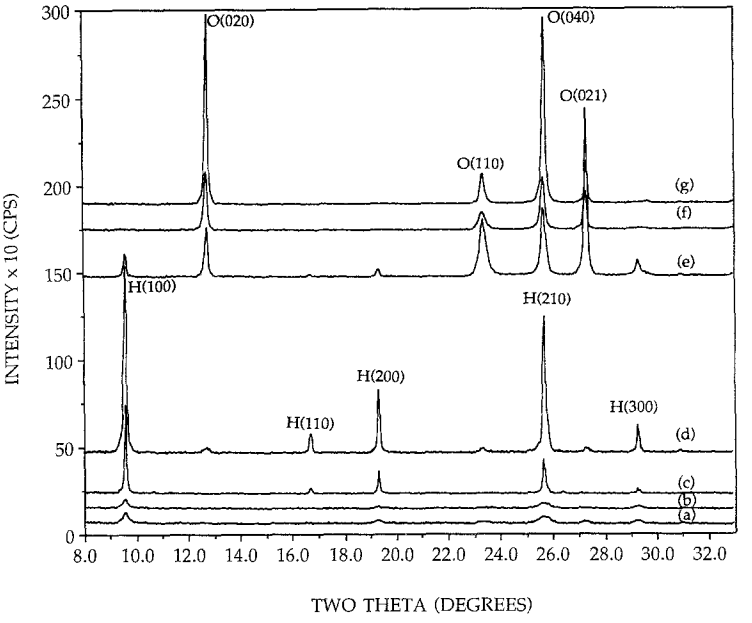

FIG. 2. XRD patterns of calcined 36.5 wt% supported and unsupported MoO_3: (a) 300°C calcined supported basic precursor (hexagonal); (b) 300°C calcined supported neutral precursor (hexagonal); (c) 300°C calcined supported acid precursor (hexagonal); (d) 300°C calcined unsupported acid precursor (hexagonal); (e) 300°C calcined unsupported basic precursor (orthorhombic and some hexagonal); (f) 300°C calcined unsupported neutral precursor (orthorhombic); (g) 500°C calcined supported neutral precursor (orthorhombic).

X-ray diffraction patterns for the unsupported and supported precursors calcined at 300 or 500°C are shown in Fig. 2. All of the three different unsupported precursor phases formed orthorhombic MoO_3 after a 500°C calcination. Only the pattern which resulted from the neutral pH precursor, $(NH_4)_6Mo_7O_{24} \cdot 4H_2O$, is shown (Pattern (g)); the others are identical. Additionally, the unsupported neutral pH and the basic precursors largely formed the orthorhombic phase upon a 300°C calcination (Patterns (f) and (e)), though a small amount of the hexagonal phase was also seen for the basic precursor. The peak breadths of the orthorhombic phases produced at 300°C are somewhat broader than those formed at 500°C, meaning that they are more poorly crystallized. The unsupported and supported hexagonal precursor phases maintained the hexagonal phase after the calcination (Patterns (d) and (c), respectively), but sintered somewhat, as the peak breadths have reduced in Fig. 2 relative to Fig. 1. Finally, the 300°C calcination of the neutral and basic precursor phases resulted in a relatively very dispersed hexagonal phase. The crystallite size of the fraction of crystallites observable by XRD was estimated from the Scherrer equation to be 320 Å, using the full width at half maximum of the unsupported phases as standards for instrumental broadening. However, since the integrated intensities of the dispersed phase are well below those of the sintered phases, a good portion of the material also exists as very small (<40 Å) particles beyond the detection limit of XRD. These could be truly amorphous or microcrystalline. No material was lost through volatilization; a high degree of crystallinity can be reestablished in the dispersed samples by subsequent high temperature treatments as will be shown in later figures.

Samples in which AHM powder was not thoroughly mixed with SiO_2 before or after the addition of water yielded the orthorhombic phase and not the well dispersed hexagonal after a 300°C calcination. Proximity to the silica surface is thus necessary for the hexagonal phase to be produced; a pH change of the liquid impregnant solution caused by SiO_2 is not a sufficient explanation.

The dispersion of the supported hexagonal MoO_3 phase, produced by a 300°C calcination, was compared to that of the supported orthorhombic phase, produced at 500°C, by treating a series of increasingly loaded samples at the respective calcination temperatures, and observing the MoO_3 loading at which crystallinity is first evidenced by XRD. The results from these experiments are shown in Fig. 3A, for the 500°C calcination, and Fig. 3B for the 300°C calcination. The weight percent loading at which the orthorhombic phase is observed is 8.8 wt%, which translates to a surface loading of 1.1 atom Mo/nm^2 and is in good agreement with the average of reported values (Table 1) of 1.1 atom/nm^2. However, the weight percent loading at which hexagonal crystallites are detected is 26.7 wt% (4.0 atom Mo/nm^2). There is the possibility that the particles are not well dispersed, but are X-ray transparent amorphous particles. However, the TEM studies presented later confirm that spreading and not the growth of an amorphous phase is the cause for the decrease in X-ray peak intensities. These two series of catalysts, analyzed on the same X-ray instrument, definitively illustrate a lesser degree of crystallinity for the hexagonal samples compared to the orthorhombic samples. The surface loading for the onset of crystallinity as detected by XRD is about 4 times higher for the well dispersed hexagonal phase than for the orthorhombic samples.

The interconversion between the hexagonal and orthorhombic phases for 26.7 wt% samples, is illustrated in Fig. 4, starting with the dispersed hexagonal phase (Pattern (a)). After an additional 4 hr of calcination at 300°C (Pattern (b)), the small hexagonal peaks had diminished completely. In some trials, however, the small peaks observed after 2 hours (as in Pattern (a)) remained after 6 hr calcination time. This may again be an effect of the thoroughness of mixing of the sample. The pattern of the orthorhombic phase which forms upon a direct, 500°C calcination for 2 hr is shown in Pattern (c); an additional 4 hr calcination at 500°C heightens the peaks by about 5 or 10%. The well dispersed hexagonal phase is converted to the sintered orthorhombic upon calcination at 500°C (Pattern (d)), and again continued calcination for 4 hr at 500°C increases the peak heights only slightly. Pattern (e), which exhibits the same sintered orthorhombic pattern and intensity as Patterns (c) and (d), was taken after a 300°C, 6 hr calcination of the sintered orthorhombic phase (as in Pattern (c)) and shows that the hexagonal–orthorhombic phase transition for the supported phases is irreversible in air, as reported for unsupported compounds (*54–56*).

The same set of calcinations were performed with the basic (monoclinic plus triclinic) precursor, with virtually the same results. That is, the crystalline phases, peak breadths, and intensities produced by the neutral and basic precursors are essentially the same upon calcination at or above 300°C.

The fraction of MoO_3 in the hexagonal and orthorhombic phase observable by XRD was found from the experiment illustrated in Fig. 5. Pure hexagonal MoO_3 was mixed to 26.7 wt% with SiO_2 powder (Pattern (a)). The acid impregnated and 300°C calcined hexagonal sample is shown in Pattern (b). While the peaks heights are somewhat lower, they are also broader; the integrated areas are equal, meaning that virtually all the sintered hexagonal phase is observed by XRD. In contrast, almost all of the well dispersed hexagonal phase (Pattern (c)) is below the limit of detection of XRD. A 26.7 wt% physical mixture of orthorhombic

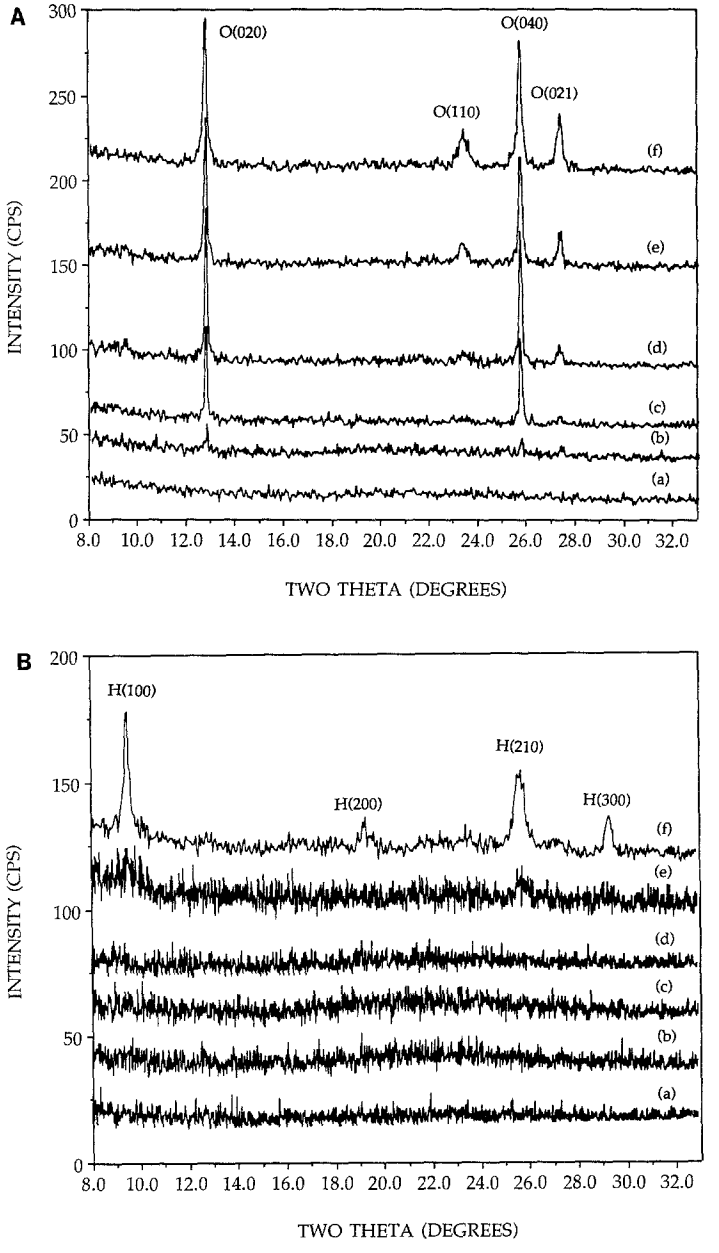

FIG. 3. (A) XRD patterns of various loadings of AHM calcined at 500°C (orthorhombic MoO_3: (a) 4.6 wt% (0.53 atom Mo/nm^2); (b) 8.8 (1.1); (c) 12.6 (1.6); (d) 16.3 (2.1); (e) 26.7 (4.0); (f) 35.3 (6.0). (B) XRD patterns of various loadings of AHM calcined at 300°C (hexagonal MoO_3): (a) 4.6 wt% (0.53 atom Mo/nm^2); (b) 8.8 (1.1); (c) 12.6 (1.6); (d) 16.3 (2.1); (e) 26.7 (4.0); (f) 35.3 (6.0).

MoO_3 + SiO_2 is shown in Pattern (d), and a 26.7 wt% impregnated orthorhombic sample in Pattern (e). The integrated intensities of the impregnated sample are about 90–95% of those of the physically mixed sample, meaning that the vast majority of MoO_3 is observable by XRD. Thus XRD provides a good measure of the difference in dispersion of the two phases, and this difference is quite large.

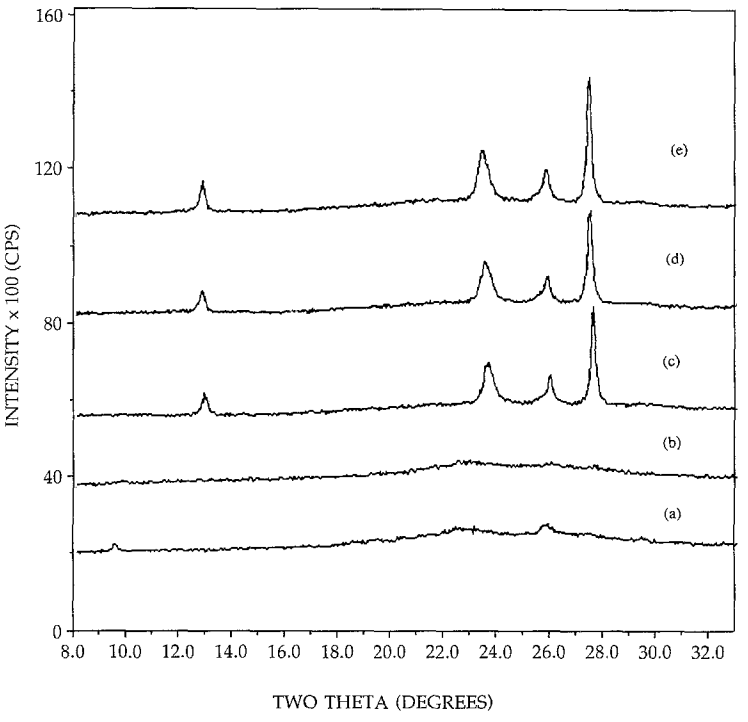

FIG. 4. XRD patterns of 26.7 wt% MoO_3, calcinations of: (a) 300°C, 2 hr; (b) 300°C, 6 hr; (c) 500°C, 2 hr; (d) 300°C, 6 hr + 500°C, 2 hr; (e) 500°C 2 hr, 300°C, 6 hr.

The dramatic effect of ammonia on the dispersion of silica supported MoO_3 was found in a series of experiments with physical mixtures of silica and hexagonal MoO_3 (formed by the acid precursor and 300°C calcination) and orthorhombic MoO_3. The first experiment is shown in Fig. 6A, for the physically mixed hexagonal MoO_3 + SiO_2. Pattern (a) was taken from the initial mixture. Upon continued calcination at 300°C (2, 4 hr, Patterns (b) and (c)) the morphology remained stable. However, when the initial sample was reimpregnated to incipient wetness with a solution containing 5 *N* NH_4OH, dried at room temperature, and calcined 2 hr at 300°C, drastic spreading occurred (Pattern (e)).

The behavior of a physically mixed silica and orthorhombic sample is shown in Fig. 6B. The orthorhombic MoO_3 for these samples was prepared by an acid impregnation of AHM and calcination at 500°C. The acid was employed to make the preparation conditions otherwise identical to the physically mixed hexagonal sample. Similar to the hexagonal MoO_3 + SiO_2 physical mixture, the pattern of orthorhombic MoO_3 was unchanged after an air calcination at 300°C of 2 hr (Pattern (b)) and was slightly diminished in intensity after 4 hr calcination time (Pattern (c)). After reimpregnation of the initial sample with the 5 *N* ammonia solution, drying, and another 300°C, 2 hr calcination as before, not only was spreading again drastic, but the majority of the observable crystalline phase was present in the hexagonal form. The final degree of crystallinity of both samples, Figs. 6A and 6B, approaches that of the dispersed, neutral and basic impregnated (thoroughly mixed) precursors (Figs. 1–5). While there are small amounts of orthorhombic remaining, this morphology will also be referred to as the "well dispersed hexagonal" phase.

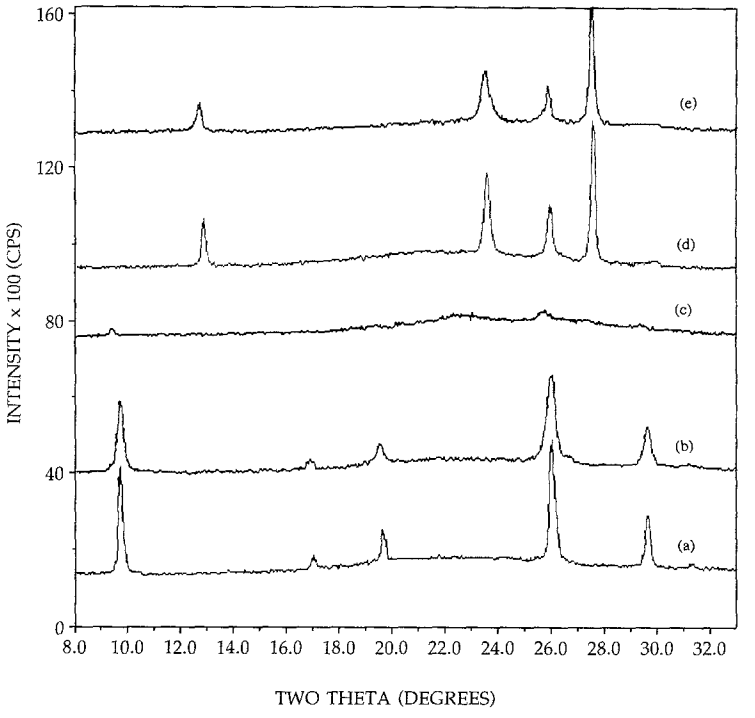

FIG. 5. XRD patterns of 26.7 wt% MoO_3: (a) hexagonal MoO_3 + SiO_2; (b) hexagonal MoO_3/SiO_2, 300°C calcination (acid impregnation); (c) hexagonal MoO_3/SiO_2, 300°C calcination (neutral impregnation); (d) orthorhombic MoO_3 + SiO_2; (e) orthorhombic MoO_3/SiO_2.

In Fig. 6C, the physically mixed orthorhombic and silica sample (Pattern (a)) shows little or no change in morphology upon continued calcination at 500°C (Patterns (b) and (c)), in agreement with similar experiments (*10, 13, 15, 16*). After impregnation with ammonia solution and a 500°C, 2 hr calcination, some peak broadening was observed (Pattern (d)), but no conversion to the hexagonal phase was evidenced.

The reversibility of MoO_3 wetting of silica via ammonia reimpregnation and the hexagonal to orthorhombic phase change were examined in a further XRD experiment. In Fig. 7, the physically mixed orthorhombic MoO_3 + SiO_2 mixture is again shown, Pattern (a), and the redispersed morphology formed by ammonia impregnation and a 300°C, 2 hr calcination is shown in Pattern (b). A 500°C, 2 hr calcination produces the sintered orthorhombic phase once again, with no hexagonal phase remaining, Pattern (c), while a second ammonia impregnation and 300°C calcination produces the dispersed mixture of phases again, Pattern (d). In another experiment not shown, distilled water was used in place of an ammonia solution in an attempt to redisperse orthorhombic MoO_3. Without ammonia, however, no change occurred. Thus, the redispersion and sintering processes are reversible contingent upon the presence of ammonia. In an attempt to remove the ammonia from a well dispersed sample, a portion of this catalyst was reimpregnated with nitric acid, and then calcined at 300°C for 2 hr. The resulting pattern is shown as Pattern (e); some sintering had been induced by the acid treatment.

Finally, the redispersion mechanism of the sintered hexagonal and orthorhombic phases was investigated by preparing XRD samples of the ammonia reimpregnated samples just after drying. These are shown

in Fig. 8. Reimpregnation of unsupported orthorhombic MoO_3 yields the ammonia rich mixture of monoclinic and triclinic phases (Pattern (a)). This sample was diluted (physically mixed) to 26.7 wt% with silica; the diluted pattern is shown in Pattern (b). Next, a 26.7 wt% physical mixture of hexagonal MoO_3 + SiO_2 was reimpregnated with ammonia and dried. It is shown in Pattern (c). The pattern is mainly monoclinic, and degree of crystallinity of this sample is lower than that of the 26.7 wt% sample in Pattern (b). Reimpregnation of pure hexagonal MoO_3 with ammonia led again to the ammonia rich monoclinic and triclinic precursors (Pattern (d)), although the ratio of the monoclinic to triclinic material is higher. A 26.7 wt% diluted sample is shown in Pattern (e), and an ammonia reimpregnated physical mixture of hex MoO_3 + SiO_2 is shown in Pattern (f). Again the pattern is mostly monoclinic, and the degree of crystallinity of the reimpregnated physical mixture is less than that of the reimpregnated-then-diluted sample.

These data indicate that the equilibrium form of MoO_3 subjected to an ammonium solution and dried at 25°C is the ammonia rich precursor phases. The SiO_2 supported samples are mainly monoclinic, while small amounts of triclinic also form in the unsupported materials. The reammoniation of anhydrous orthorhombic MoO_3 to this extent has not been reported, although hexagonal MoO_3 has been produced from mixing Mo $O_3 \cdot 2H_2O$ with excess liquid solution con-

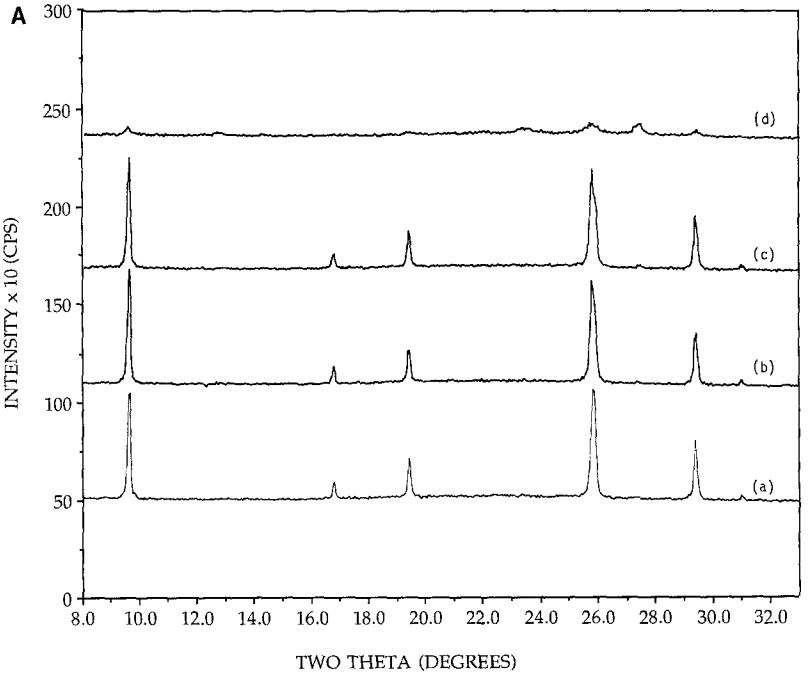

FIG. 6. (A) XRD patterns of 26.7 wt% physically mixed hexagonal MoO_3 + SiO_2: (a) initial mixture; (b) after 300°C, 2 hr calcination; (c) after 300°C, 4 hr calcination; (d) after reimpregnation with ammonia solution, calcination for 300°C, 2 hr. (B) XRD patterns of 26.7 wt% physically mixed orthorhombic MoO_3 + SiO_2: (a) initial mixture; (b) after 300°C, 2 hr calcination; (c) after 300°C, 4 hr calcination; (d) after reimpregnation with ammonia solution, calcination for 300°C, 2 hr. (C) XRD patterns of 26.7 wt% physically mixed orthorhombic MoO_3 + SiO_2: (a) initial mixture; (b) after 500°C, 2 hr calcination; (c) after 500°C, 4 hr calcination; (d) after reimpregnation with ammonia solution, calcination for 500°C, 2 hr.

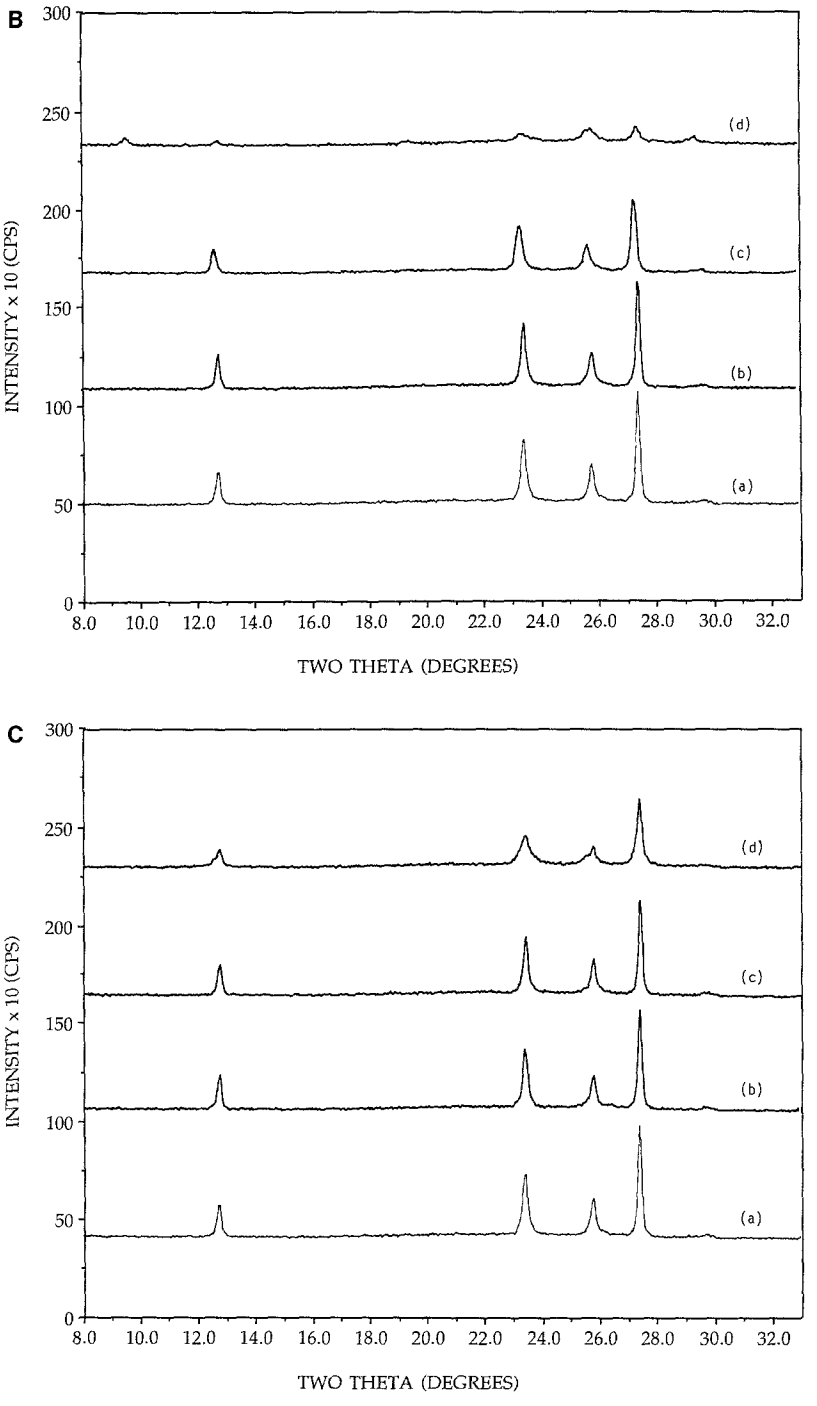

FIG. 6.—*Continued*

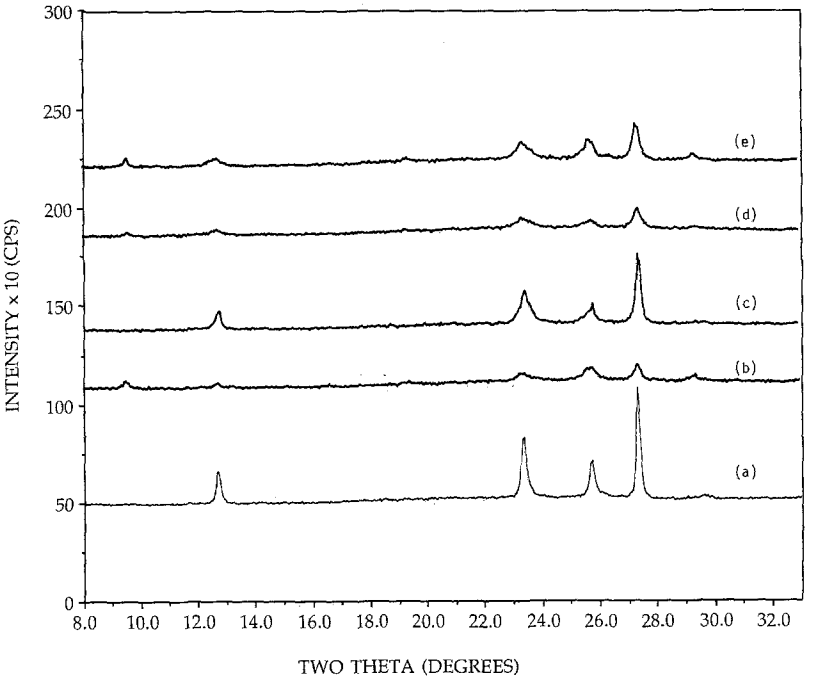

FIG. 7. XRD patterns of 26.7 wt% supported MoO_3: (a) 500°C calcined, orthorhombic MoO_3/SiO_2; (b) ammonia reimpregnated and 300°C calcined; (c) 500°C calcined; (d) ammonia reimpregnated and 300°C calcined; (e) acid impregnated sample, 300°C calcined.

taining NH_4Cl (*54*). The pathway from the sintered hexagonal or orthorhombic phases to the well dispersed hexagonal phase, as seen in Figs. 6A and 6B, appears at least in part to pass through the basic precursor phase. From there it becomes parallel to decomposition of the impregnated basic precursor.

Transmission Electron Microscopy Characterization of Model Catalysts

An ammonium molybdate precursor, deposited onto a planar substrate by allowing a drop of 2×10^{-3} molar solution to dry at room temperature on the substrated grid, is shown in Fig. 9A just after drying. This precursor was mainly in the form of very large bundled aggregates, with a number of maller such aggregates, one of which is labeled "C" in the figure. After a 500°C calcination, the precursor had spread dramatically (Fig. 9B). A higher magnification image of region "C" from Fig. 9A is shown in Fig. 9C before calcination, and in Fig. 9D after calcination. The original material almost completely disintegrates, leaving only three smaller crystallites. These exhibit aprons of surrounding material. In addition, patches of material appeared over the substrate. These did not diffract, and neither was a third dimension apparent upon changing the sample orientation, meaning that the patches were thin. These 100 to 400 Å patches are somewhat similar to small, ill defined MoO_3 patches observed on alumina (*60*), although larger in size. This behavior implies that the material can drastically spread as the precursor transforms to the trioxide. This change in morphology could likely have occurred during the warmup to 500°C. Appreciable migration of material was observed in another TEM study as a supported Mo metal and Mo suboxide sam-

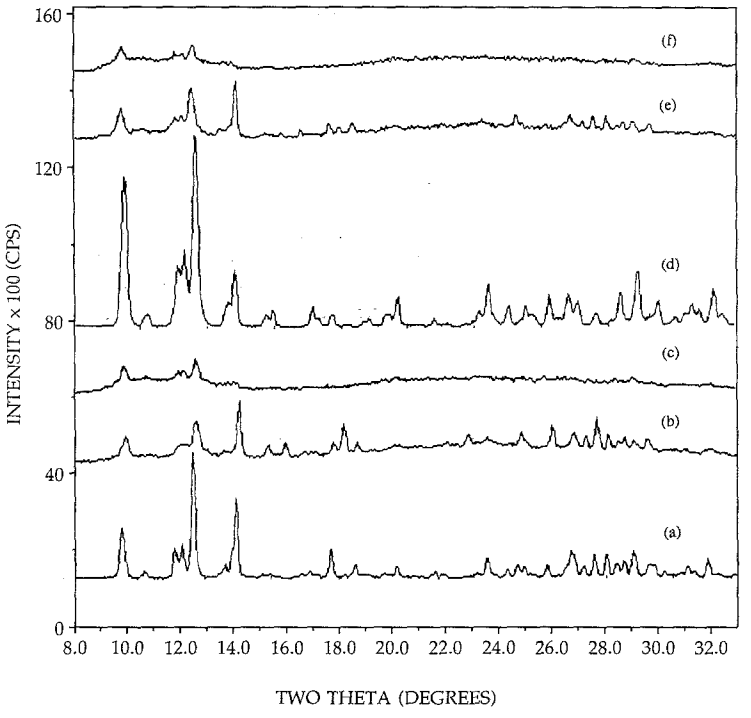

FIG. 8. XRD patterns of ammonia reimpregnated, dried samples: (a) unsupported orthorhombic MoO_3; (b) sample (a) after dilution with SiO_2 to 26.7 wt%; (c) reimpregnated physical mixture of orthorhombic MoO_3 + SiO_2; (d) unsupported hexagonal MoO_3; (e) sample (d) after dilution with SiO_2 to 26.7 wt%; (f) reimpregnated physical mixture of hexagonal MoO_3 + SiO_2.

ple was transformed to trioxide by heating from 200 to 300°C in air (*61*).

The dispersion of the hexagonal phase and its conversion to the orthorhombic is illustrated in Fig. 10. The very large crystallite attached to the silica sphere in Fig. 10A was produced by a 300°C, 2 hr air calcination. It was found to be hexagonal from an analysis of its spot electron diffraction pattern. Most of the area of the silica sphere was empty. After an additional 300°C, 4 hr calcination, shown in Fig. 10B, most of the MoO_3 appeared to have dispersed over the silica sphere. This finding supports the conclusion that the hexagonal phase disperses over the silica surface. (An opposing explanation of the previous XRD results showing low intensity of the hexagonal phase would be that the 300°C phase is poorly dispersed but amorphous, which would also be X-ray transparent.)

Figures 10A and 10B illustrate the further dispersion of the highest loading hexagonal MoO_3 XRD sample in Patterns (a) and (b) of Fig. 4. The remaining multigrained cluster in Fig. 10B appears to wet the silica surface. Upon a 500°C calcination for 2 hr, the crystallite cluster's volume decreased somewhat further and individual grains in it appeared to have sintered together. The sintered crystallite would produce a sharper XRD peak, while the multigrained aggregate in Fig. 10B would produce a peak of similar integrated intensity, but of smaller height and greater breadth. The area was not monitored after further calcination time to see whether the orthorhombic crystallite grew more in size. As another indication of a weaker MoO_3/SiO_2 interaction, however, a smooth junction of MoO_3 with the silica surface is no longer apparent in Fig. 10C; it does not appear that this crystallite strongly wets the

surface. In an earlier work (*57*) the stability of the orthorhombic phase at 500°C was documented.

Transformation of the hexagonal crystallites, produced by another 300°C, 2 hr calcination of the dried precursor, Fig. 11A, into the orthorhombic form by a 500°C, 2 hr calcination is shown in Fig. 11B. The volume of the crystallite phase did increase considerably in this instance. In fact, some material appears to have come from the surrounding grid bar. Figure 11 is indicative of the many XRD sequences in which the sintered orthorhombic phase was produced from the hexagonal phase. The same trends in dispersion with respect to calcination temperature, that is, increasing dispersion during a low temperature calcination of the hexagonal phase and decreasing dispersion during a high temperature calcination of the orthorhombic phase, were reported in an earlier work (*57*).

X-ray Photoelectron Spectroscopy Characterization of Low Loading Catalysts

Precursor and calcined samples of 1.8 and 6.8 weight percent catalysts, or 0.2 and 0.8 atom/nm^2 surface loading, were characterized with XPS. For each loading, two initial pH values were used, one below the point of zero charge of silica, where strong adsorption of negatively charged molybdate ions can occur over a positively charged silica surface (*1–9*), and the other over a pH of 9, far above the pzc and so over a negatively charged silica surface. After the impregnation and drying at 40°C for 2 hr in a rotary vacuum drier, samples were calcined at both 300 and 500°C for 2 and 6 hr. Mo dispersion was estimated by the Mo/Si ratio; this is charted as a function of initial pH, calcination temperature, time, and loading in Fig. 12. For both loadings the initial dispersion of the high pH sample was much higher than the low pH sample: a factor of almost 2.5 higher for the 0.2 atom/nm^2 sample, and over 5 times higher for the 0.8 atom/nm^2 sample. In every case, the dispersion of the highly dispersed samples decreased upon calcination, while that of the poorly dispersed precursors increased upon calcination. Because the final dispersion is below maximum, the "patchy monolayer" morphology is evidenced in all of the calcined samples.

The final dispersion for the respective weight loadings appeared to be almost independent of initial dispersion, and only a weak function of calcination temperature. For the high loading catalyst, the Mo/Si ratio of the 500°C calcined samples is about 20% higher than the average final Mo/Si ratio of the 300°C calcined sample, 32×10^{-3} to 25×10^{-3}. The average final Mo/Si ratios of the lowest loading samples are about the same, 8×10^{-3}. The final surface compositions are roughly proportional to loading. These results support the earlier TEM experiment (Fig. 9) which shows that drastic rearrangement of material can occur in the conversion from precursor to trioxide.

DISCUSSION

Equilibrium Phase Model for Silica Supported MoO_3

A summary of the various phases produced by calcinations of the unsupported, high loading supported and low loading supported catalysts is shown in Fig. 13. In the series of unsupported materials, Fig. 13A, the acid precursor which resulted in a hexagonal precursor at room temperature after drying remained in this phase after a 300°C calcination and formed the orthorhombic phase at 500°C (Figs. 1 and 2). However, even at 300°C the neutral precursor con-

FIG. 9. TEM micrographs of calcined MoO_3/planar SiO_2: (A) AHM impregnated, dried; (B) sample (A) calcined at 500°C, 2 hr; (C) closeup region of dried sample; (D) closeup of same region as (C) in calcined sample.

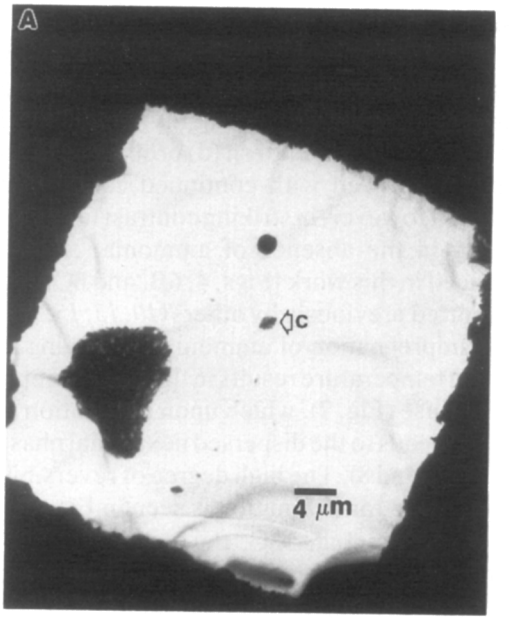
A
C
4 μm

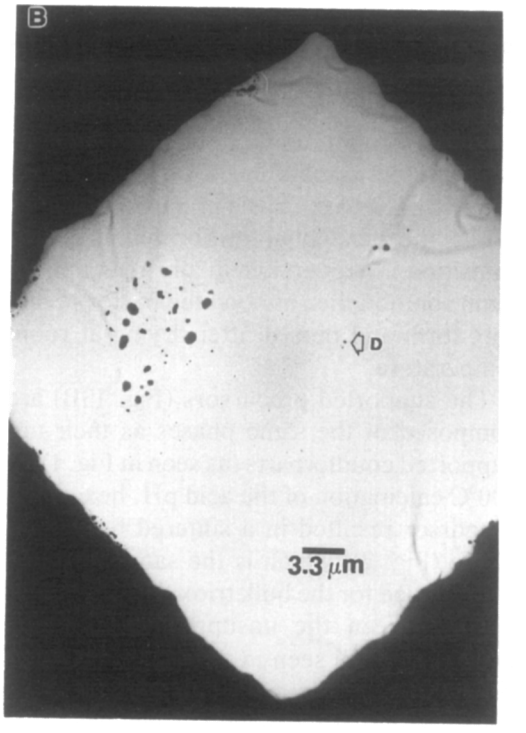
B
D
3.3 μm

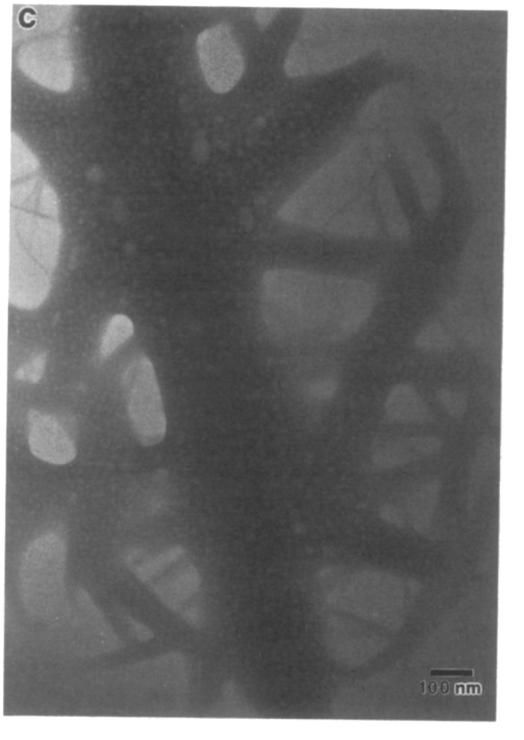
C
100 nm

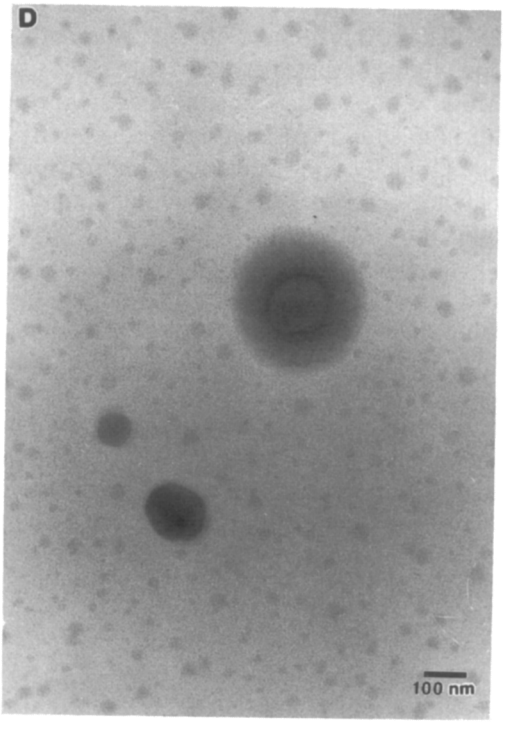
D
100 nm

verted entirely to the orthorhombic phase, and the basic precursor converted almost entirely to the orthorhombic phase (Fig. 2). With this reimpregnation of ammonia and drying at room temperature, the unsupported orthorhombic and hexagonal samples convert back to the basic precursor (Fig. 8). While the hexagonal–orthorhombic phase transition is irreversible in air, in an ammonium solution the ammoniated basic precursors form and persist after drying at room temperature.

The supported precursors (Fig. 13B) are composed of the same phases as their unsupported counterparts (as seen in Fig. 1). A 300°C calcination of the acid pH, hexagonal precursor resulted in a sintered hexagonal phase (Fig. 2), which is the same behavior as observed for the bulk trioxide. The difference between the unsupported and supported forms is seen in the behavior of the neutral and basic precursors calcined at 300°C. Whereas the unsupported forms convert totally or almost totally to the orthorhombic phase, the supported forms convert to a well dispersed hexagonal phase (Fig. 2). (The orthorhombic phase also results at 300°C if contact between the silica and MoO_3 is not good.) Thus there are two equilibrium supported phases produced by a 300°C calcination. One, the sintered hexagonal phase, forms with an acid impregnation, and the other, the dispersed hexagonal phase, forms from an impregnation at neutral pH or in the presence of ammonia. The sintered hexagonal phase is metastable in that once it is reimpregnated with ammonia and forms the basic precursor phase, further calcination can only lead to the sintered orthorhombic phase (when performed at the higher temperature). An acid treatment of the dispersed hexagonal phase and a 300°C calcination leads to the formation of a mixture of sintered orthorhombic and hexagonal crystallites (Fig. 8) and not to a pure sintered hexagonal phase.

At 500°C the one and only thermodynamically stable supported phase is the sintered orthorhombic. (The slightly broadened peaks in Fig. 6C, Pattern (d) probably would have narrowed with continued calcination time.) However, in striking contrast to its stability in the absence of ammonia, as evidenced in this work (Figs. 4, 6B, and 6C) and reported previously by others (*10, 13, 15, 16*), a reimpregnation of ammonia and drying at room temperature results in the basic precursor phase (Fig. 7), which upon calcination at 300°C leads to the dispersed hexagonal phase (Figs. 6 and 8). The high degree of reversibility of this transformation is seen in Fig. 8.

Finally in Fig. 13C, the "patchy monolayer" morphology is shown in low loading catalysts arising from either a poor or good initial dispersion of the precursor. In Fig. 12, the poorly dispersed sample spread and the highly dispersed sample sintered upon calcination at 300 or 500°C, attaining approximately the same degree of dispersion. The final morphology of the MoO_3 in these low loading catalysts appears to be independent of the initial precursor dispersion. In fact, the morphologies of all loadings of silica supported MoO_3 appear to arise as thermodynamically stable or metastable phases. Ammonia appears to be a key link between these states, as will be discussed later. Figure 13 represents a crude equilibrium phase model for silica supported MoO_3 phases.

Low Loading Catalysts

For the low loading catalysts, there are two factors which might be used to explain the trends in initial (precursor) dispersion versus pH; these are the surface charge on silica and the type of Mo ionic complex present in the liquid solution. The pH of near 1.4 was chosen in this work to be below the pzc

FIG. 10. TEM micrographs of calcined MoO_3/nonporous spherical SiO_2: (A) AHM impregnated, calcined 300°C, 2 hr; (B) sample (A) calcined an additional 4 hr; (C) sample (B) calcined at 500°C, 2 hr.

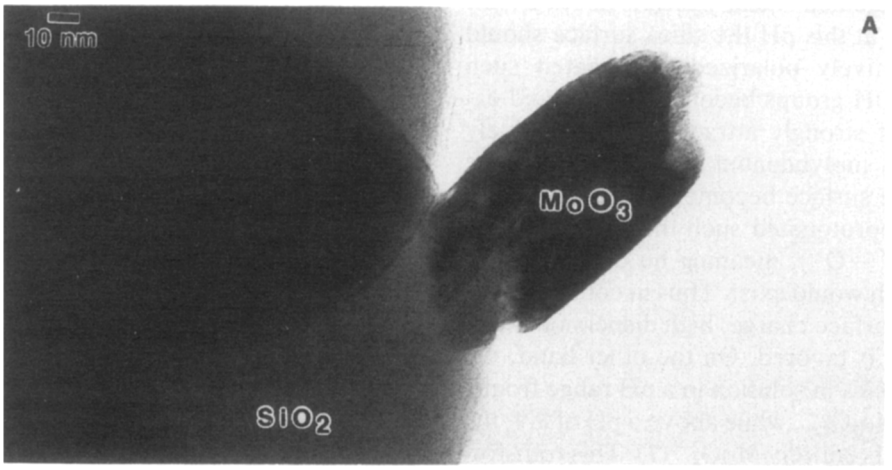
10 nm
A
MoO3
SiO2

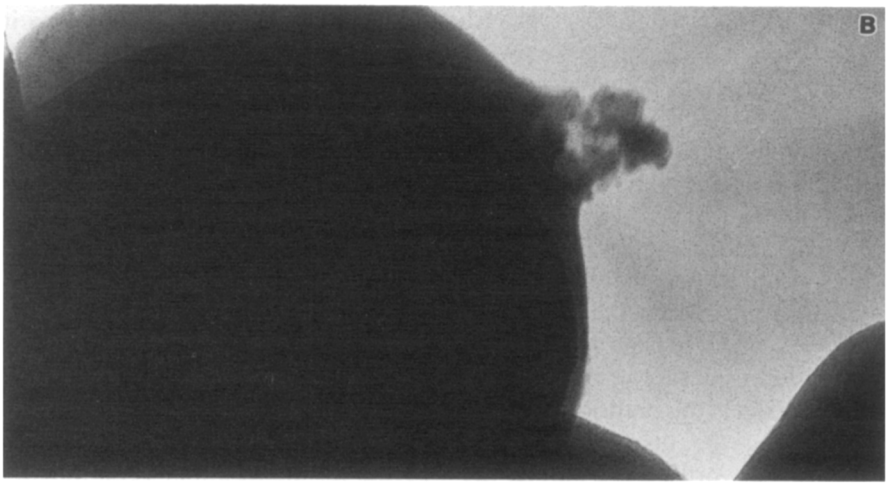
B

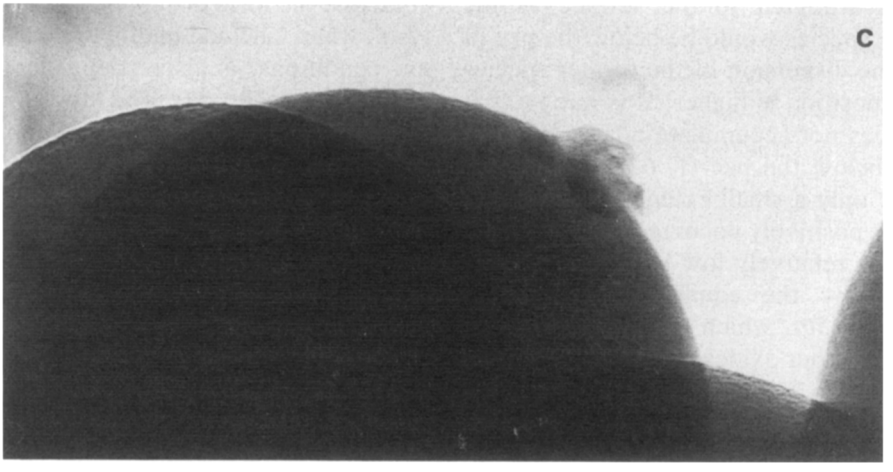
C

of noncalcined silica, which is about 2 (*62*). That is, at this pH the silica surface should be positively polarized (protonated such that $-OH$ groups become $-OH_2^+$) and capable of strongly attracting the negatively charged molybdenum species. Above the pzc, the surface becomes negatively polarized (deprotonated such that $-OH$ groups become $-O^-$), meaning no coulombic interaction would exist. Thus in consideration of the surface charge, high dispersion at the low pH is favored. On the other hand, the Mo species in solution in a pH range from 2 to 6 is $Mo_7O_{24}^{6-}$, while above a pH of 8.9, the species is entirely MoO_4^{2-} (*1*). This transformation is written as

$$Mo_7O_{24}^{6-} + 4H_2O \leftrightarrow 7MoO_4^{2-} + 8H^+.$$

Thus consideration of the liquid phase speciation would have it that the higher pH preparation would yield a higher dispersion.

In these samples the pH of the liquid phase was known, as an excess of liquid was used precisely so that pH could be measured and controlled (were dry impregnation used, the liquid pH would be considerably altered by the solid since the mass percent of oxide is so high (*63, 64*). The present results support the second consideration, that the liquid phase speciation is the predominate factor in determining the dispersion of the precursor. In other words, even though the MoO_4^{2-} species present at high pH is not as strongly attracted to the surface as the $Mo_7O_{24}^{6-}$ species would be below the pzc of silica, the dispersion of the former species after deposition is higher. It is known that silica does not accumulate a large positive charge below the pzc (*1, 62*), which is to say that only a small extent of the surface becomes positively polarized. This is apparent in the relatively low loadings of MoO_3 obtained by the equilibrium adsorption method (*1, 50*), which are well below the values for other oxides such as alumina and titania (*1*).

Results from a study of MoO_3 adsorption over alumina with Raman spectroscopy (*65*) are similar: higher dispersion was reported for an impregnation at an initial pH of 11, in which the MoO_4^{2-} species was present in the liquid phase, compared to an initial pH of 6, below the pzc of alumina. That is, no peaks corresponding to bulk MoO_3 were detected at the higher pH, but were detected at the lower pH. Actually, the final solution pH in this system would be influenced by the solid (*64*) and would be less than 11 on the high side and more than 6 on the low side, perhaps even approaching the pzc of alumina (which is 7–9 (*62*)) from both directions. However the higher dispersion of the high pH sample does appear to have resulted from the liquid phase speciation and not the surface charge, as was the case in the present results.

In spite of the great differences in initial dispersion, however, after calcination the dispersion of MoO_3 in the low loading catalysts is almost the same and is also not a strong function of calcination temperature. The increases in dispersion of material during calcination, even at 500°C, are seen with both XPS (Fig. 12) and TEM (Fig. 9). This would imply that the precursor phases are highly mobile, and much movement occurred in the initial stages of the calcination, presumedly during the warmup.

That only one equilibrium dispersion is produced over silica, independent of initial precursor distribution, compliments the recent *in situ* Raman works (*33–36, 49*), which state that the form of supported MoO_3 catalysts, when calcined and hydrated at ambient conditions, is also independent of the preparation technique. The $Mo_7O_{24}^{6-}$ species predicted over silica may correspond to the less than perfectly dispersed phase observed in the present work. While the 0.8 Mo/nm^2 catalyst is above the limit at which microcrystals have been observed by Raman, a relatively small amount of crystalline material at this loading (*35*) should affect dispersion insignificantly. At sufficiently low loadings where insignificant amounts of bulk MoO_3 form, it is reasonable to expect that both the form of the Mo species and Mo dispersion follow the same trends.

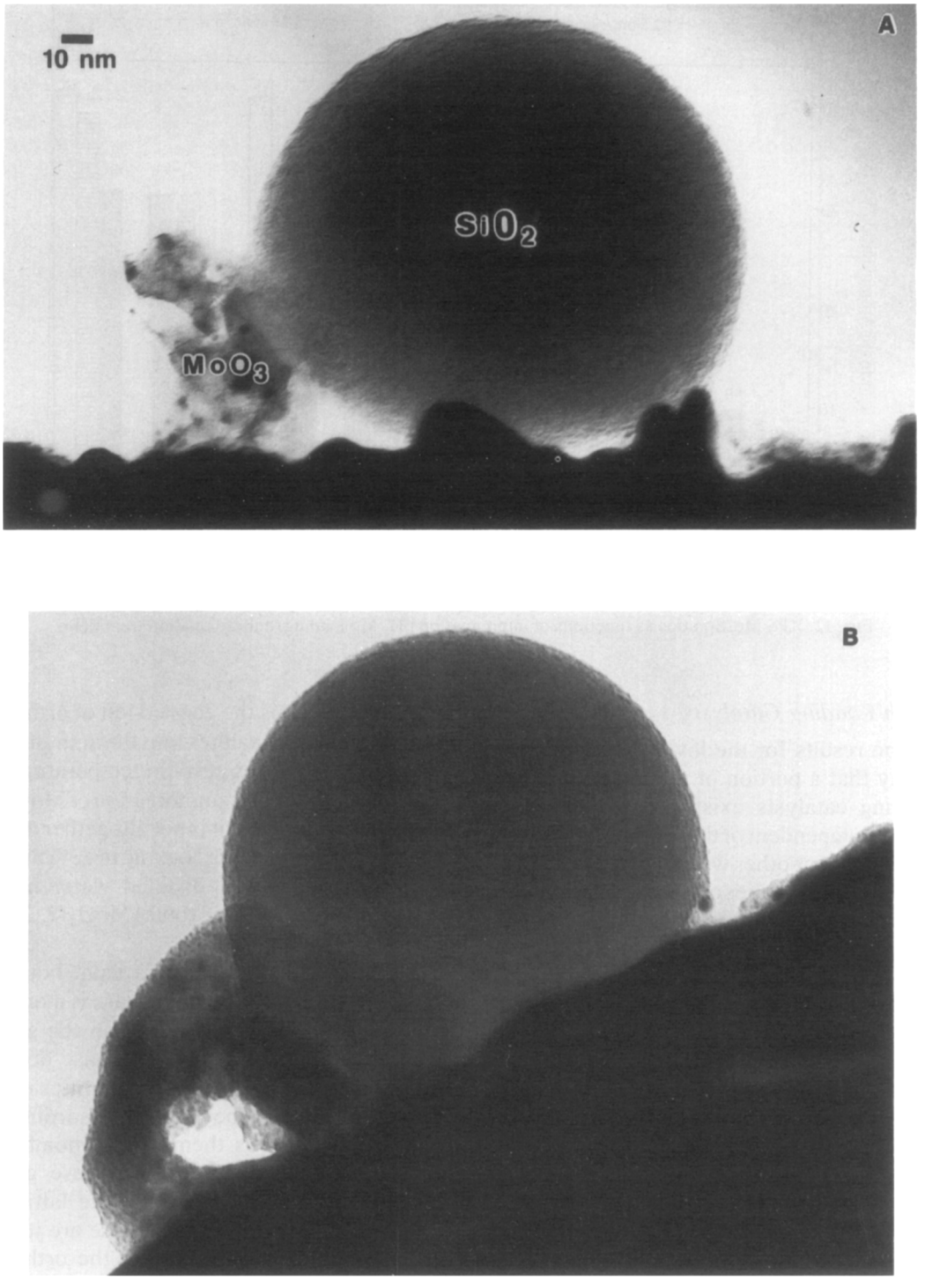

FIG. 11. TEM micrographs of calcined MoO_3/nonporous spherical SiO_2: (A) AHM impregnated, calcined 300°C, 2 hr; (B) sample (A) calcined at 500°C, 2 hr.

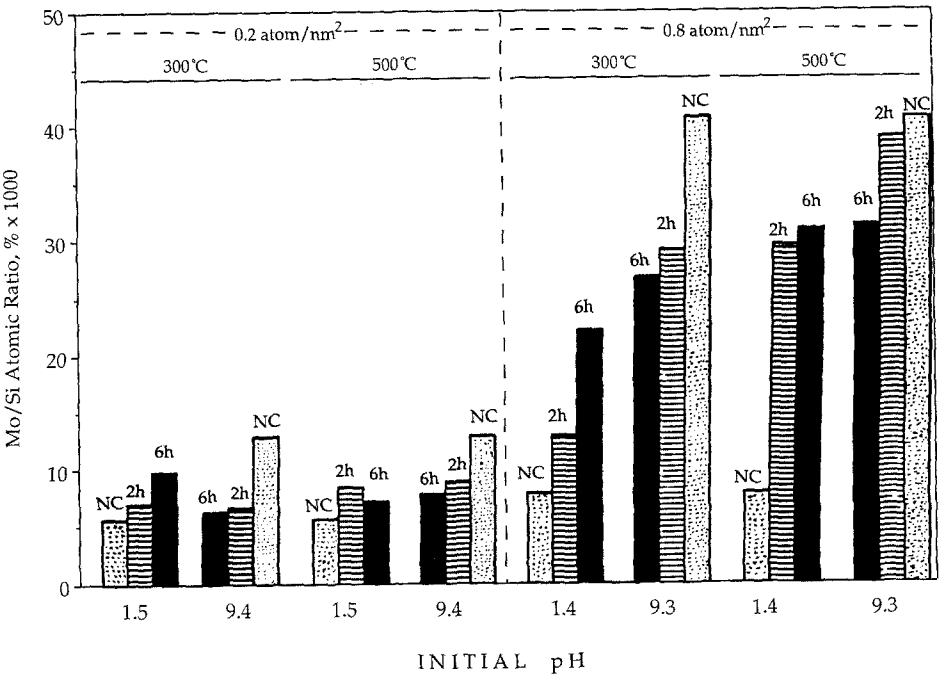

FIG. 12. XPS Mo/Si ratios as functions of impregnation pH, Mo loading, and calcination treatments.

High Loading Catalysts

The results for the low loading catalysts imply that a portion of the material in high loading catalysts exists in well dispersed form, independent of the morphology of bulk crystallites or other well dispersed material. The lower intensities of XRD peaks of the impregnated orthorhombic sample and the broadened peaks of the impregnated hexagonal sample compared to the physically mixed samples in Fig. 5 bear this out to some extent. The amount of well dispersed material appears to be lower in these samples than in the low loading catalysts, though. This may imply that once MoO_3 crystallites form in large quantity, MoO_3 units prefer to sinter onto them rather than to remain attached to the silica surface. There is insufficient surface characterization on the high loading samples to ascertain this.

The role of ammonia in the redispersion behavior of silica supported MoO_3 will now be addressed. One definite role of ammonia in the production of the well dispersed hexagonal morphology is the conversion of orthorhombic MoO_3 crystallites into the ammonia rich precursor phases at room temperature. While this extensive reammoniation of MoO_3 has not been reported, it is not altogether unexpected, as a process of soaking in a 3% ammonia solution and/or distilled water has been used to dissolve free (bulk) MoO_3 (*2*, *24*, *37*, *66*) from oxide surfaces.

The absorption of ammonia from liquid solution by the orthorhombic phase is markedly different from its behavior in the gas phase. Whereas the hexagonal phase does adsorb ammonia and water in quantities orders of magnitude beyond physisorption (*67*) (and so *ab*sorbs them), orthorhombic MoO_3 largely does not adsorb these gas phase species (*67*). Apparently the lattice parameters of the hexagonal phase are just sufficiently larger than those of the orthorhombic phase to permit this to occur. There are several reasons why this restriction for the orthorhombic phase is overcome in the liquid phase. First, at basic pH, the MoO_3

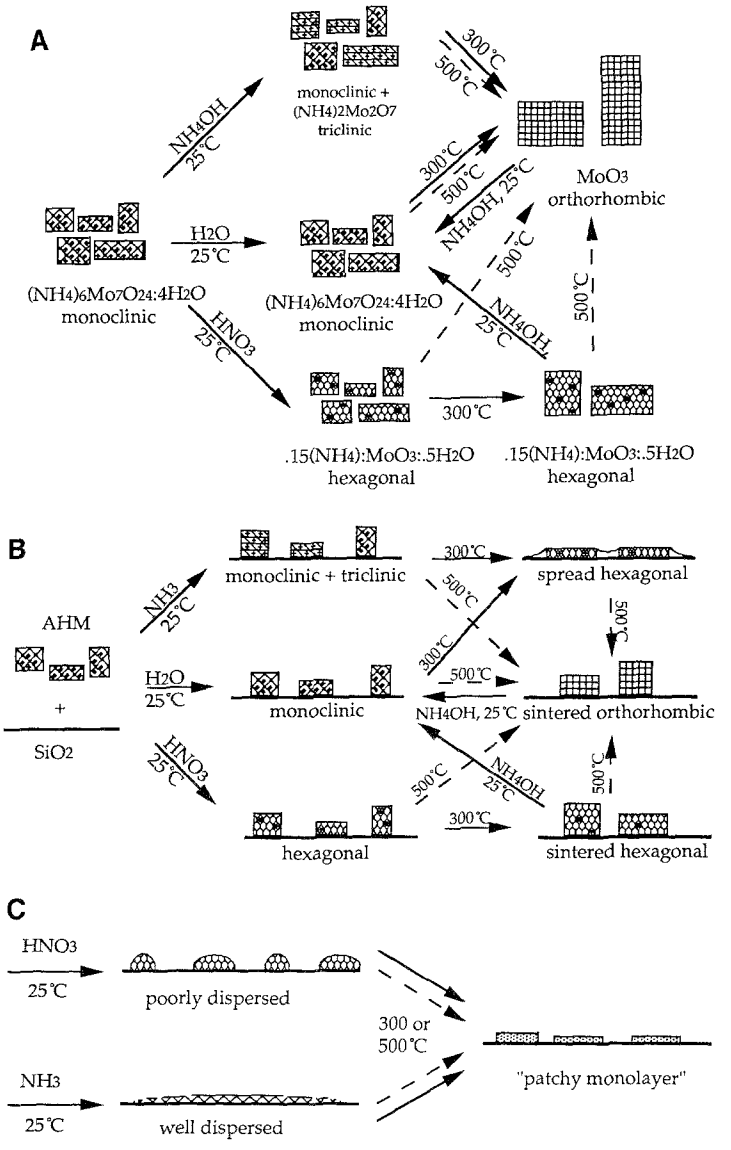

FIG. 13. Equilibrium phase model of MoO_3 containing phases supported on silica.

surface would be negatively polarized, since the pzc of MoO_3 is low (about 5.5 (*2*)), and so attractive forces would exist between the negatively charged surface and positively charged ammonium ions. Second, the ammonium ion is smaller than the ammonia molecule.

The reammoniation transformation observed for the supported phases appears to also involve some dissolution, as the degree of crystallinity of reimpregnated physical mixtures of MoO_3 + SiO_2 in Fig. 8 is less than that of physical mixtures of reimpregnated MoO_3 and SiO_2. That is, some of the material appears to have dissolved and dispersed onto the silica surface in the course of the reimpregnation of the MoO_3 + SiO_2 samples, in the manner of the high pH, low loading samples. Ammonia must be the cause of dissolution, as control reimpregna-

tions with water alone did not affect the morphology. Dissolution will occur if the concentration of ammonium hydroxide is high enough to neutralize the effect of the silica surface on the liquid phase pH, and to still maintain a pH greater than 6, where MoO_3 dissolution occurs (*2*). As about 2 ml/gm of impregnant are used, the amount of OH^- in this liquid is (5 mol/liter) × (0.002 liter) or 10^{-2} mol. On 1 g or 380 m^2 of surface there are 5 hydroxl groups/nm^2, or a total of only 3.2×10^{-3} mol. Even assuming all the hydroxyl groups dissociate, only 16% of the liquid phase OH^- will be neutralized. The final pH should be very high.

Thus, once the supported, sintered orthorhombic or hexagonal phases are reimpregnated with ammonia, the route to the formation of the well dispersed hexagonal phase becomes partly parallel to that of a calcination of supported AHM (for the fraction of material which gets converted to the monoclinic phase) and partly parallel to the formation of well dispersed, low loading precursors (for the dissolved fraction of material). The question which arises now is why the hexagonal phase formed by a calcination at 300°C has a stronger interaction with the surface than the orthorhombic phase at 500°C. At least two possibilities exist; one is a further role of ammonia in promoting a stronger MoO_3–SiO_2 interaction, and the other is the relative abundance of hydroxyl groups at the respective calcination temperatures. Does the loss of hydroxyl groups on the surface or the loss of ammonia from the hexagonal phase cause the well dispersed hexagonal state at 300°C to transform to the sintered orthorhombic state at 500°C?

The possible role of ammonia will be addressed first. The difference between the precursors which did spread on silica, and the acid precursor which did not, was the amount of ammonium ions contained in each. The NH_4^+/Mo ratio of ammonium ions in neutral and basic precursors which spread is 6 : 7 and 1 : 1, respectively. This can explain why the two precursors behave similarly. On the other hand, the amount of interstitial ammonium in the acid (hexagonal) precursor is small, the ammonium to MoO_3 ratio being at most about 0.1 : 1. Since redispersion did not occur for the hexagonal precursor, it can be said, first, that the redispersion phenomenon cannot be attributed directly to the presence of the hexagonal phase and, second, that the redispersion phenomenon is not caused solely by the presence of silica. The simultaneous presence of ammonia and silica has earlier been reported to be necessary to produce the hexagonal phase (*55*).

It has been demonstrated that a portion of the interstitial ammonia in the hexagonal phase is very stable, being released only upon the transformation to the orthorhombic phase (*54, 56, 67*). (Indeed, this phenomenon might be explained from the standpoint that the loss of ammonia triggers the phase transition.) Infrared studies of MoO_3/SiO_2 catalysts have shown that ammonia from the AHM precursor remains present in the catalyst at temperatures up to 300°C, but not at 500°C (*28, 56*). The ammonia that is present in the hexagonal acid precursor sample is strongly bound within this phase. On the other hand, as the monoclinic and triclinic precursors decompose upon their conversion to the hexagonal phase, an appreciable amount of ammonia would be released. The higher dispersion of the hexagonal phase resulting from the neutral and basic precursor phases may thus hinge on the role of excess ammonia and its interaction with the silica surface.

The other potential factor which may explain the observed differences between the dispersed hexagonal crystallites formed at 300°C and the sintered orthorhombic crystallites formed at 500°C is the degree of hydroxylation of the silica surface. The classical, widely cited mechanism for the interaction of MoO_3 with oxide surfaces during impregnation and calcination (*68*) involves the reaction of MoO_4^{2-} complexes with two hydroxyl groups. The greater capacity of alumina or titania for monolayer MoO_3 species relative to silica can be attrib-

uted to the higher concentration of hydroxyl groups on alumina (*33*).

The total number of hydroxyl groups over amorphous silica is generally thought to be in the neighborhood of 5 sites/nm^2 for an uncalcined surface at room temperature (*69–71*). Not all of these hydroxyl groups are equivalent, with three different types being reported (*70*), and in regards to the interaction with MoO_3, not all are thought to be reactive. A common method which has been employed to estimate the number of "reactive" hydroxyl groups is exchange with flourine (*7, 32*). The reported number of flourine exchangeable hydroxyl groups varies widely, from 1.9 (*7*) to 0.25 (*32*) groups/nm^2.

The total number of hydroxyl sites at 500°C appears to be diminished, on average, by about 30% with respect to the number of sites at 300°C (*69–71*). There does not appear to be data presently available on the variation of the number of "reactive" sites with temperature.

The low loading catalysts do not appear to be affected by the partial dehydration of the surface (Fig. 12); the number of reactive hydroxyl groups is probably always in excess in those samples. A qualitative correlation between dispersion and the number of hydroxyl groups does appear to hold for the high loading catalysts, but it seems questionable that the apparently drastic changes in dispersion can be caused by only a 30% change in the number of hydroxyl groups. High weight loading anchored allyl and chloride complexes maintain their high dispersion even when calcined at high temperatures (*35*); in contrast, the well dispersed hexagonal phase sinters markedly. This supports the idea that some of the MoO_3 is present in a microcrystalline phase below the limit of detection of XRD, the behavior of which does not appear to be governed by the surface hydroxyl concentration. The abundance of microcrystalline orthorhombic MoO_3 is implicated in the literature (see Table 1 and comments in the introduction); large amounts of microcrystalline hexagonal MoO_3 are not unreasonable. A final indication that the hydroxyl interaction concept is insufficient to describe the results is that the acid reimpregnated, well dispersed hexagonal sample in Fig. 8 sintered a bit after continued calcination at 300°C. The effect of the acid impregnation on the silica surface would be to bring the surface closer to its pzc, and to actually increase the number of hydroxyl groups. According to this theory, spreading would be expected. On the other hand, the acid impregnation would tend to pull NH_3 out of the trioxide matrix, as occurs in the formation of hexagonal MoO_3 from the AHM precursor. According to the ammonia interaction scheme, this would lessen the interaction with the surface and cause sintering.

The persistence of a bulk microcrystalline phase in the high loading samples explains why the high loading catalysts exhibit multiple stable morphologies while the low loading catalysts exhibit only a single stable morphology. In ammonium rich precursor crystallites, ammonium can be eliminated in two ways; thermally, and slowly at 300°C, which permits the spreading to occur and results in the dispersed morphology, or more completely in solution with acid at room temperature. In this case no excess ammonia is left to promote spreading, and the sintered hexagonal morphology persists. In low loading catalysts there is insufficient material to form bulk MoO_3 and so to store NH_4^+, so that only one morphology is possible.

A microscopic mechanism of an ammonia enhanced MoO_3–SiO_2 interaction is impossible to surmise from the experiments conducted here. Several possibilities might be suggested. One possibility is that ammonium ions in small crystallites themselves directly interact with the silica surface, perhaps with a segment of partially negatively charged hydroxyl groups of insufficient charge to have undergone the anchoring reaction, or with negatively charged terminal oxygens. Alternatively, it may be tempting to ascribe the behavior to excess NH_3 re-

leased into the hydrated layer in catalysts at ambient conditions, as was done for the precursors of the low loading catalysts. This effect would be to raise pH, causing formation of the more dispersed MoO_4^{2-} species. While the samples were equilibrated at ambient conditions prior to analysis by XRD and TEM, morphological changes occurred during the 300 and 500°C calcinations as has been documented *in situ* (*57*), meaning that equilibrium considerations in a hydrated water layer are probably inapplicable for the changes occurring during calcination. This type of mechanism might apply in some fashion inside the MoO_3 crystallites at the higher temperatures, however. Since both water and ammonia exist as interstitial impurities in the hexagonal lattice, on a very localized scale the pH may be increased, promoting the formation of the monomer-like units. The local environment would then approach those over Al_2O_3, TiO_2, or MgO, which possess much higher pzc's than silica and naturally have a higher surface pH and concentration of monomer units (*33–36*).

Any of the above mechanisms is in agreement with the consideration of spreading as an oxide–oxide wetting phenomenon (*16, 72, 73*), as has recently been invoked, for example, to contrast MoO_3 redispersion behavior over alumina and silica in a definitive Raman microscopy study (*16*). These microscopic mechanisms can all account for a global decrease in the surface free energy between the metal oxide and support, which swings the balance of surface free energy considerations to wetting.

In summary, the model suggested here for high loading catalysts is that excess ammonium ions present in the monoclinic and triclinic precursors are capable of occupying interstitial sites of microcrystalline MoO_3 during moderate temperature calcinations and in doing so enhance the MoO_3–SiO_2 interaction. This results in a "well dispersed" morphology at high loadings. Sintering at high temperature is due to loss of ammonium from the oxide framework. Ammonia reimpregnation, which leads back to the well dispersed hexagonal phase, may offer a simple regeneration process for spent Mo containing catalysts.

The supported hexagonal phases appear stable at temperatures $\leq$300°C, which is well within the temperature range employed, for example, in methanol oxidation. The highly dispersed hexagonal phase reported here may possess potential advantages compared to the orthorhombic and submonolayer forms normally employed. A comparison of the catalytic activity of all the various forms of silica supported MoO_3 is now being undertaken.

CONCLUSIONS

All morphologies of silica supported MoO_3 appear to be thermodynamically driven. At low loadings there appears to be one stable morphology and dispersion, which agrees with recent *in situ* Raman data. For high loaded calcined catalysts there appear three states: a metastable sintered hexagonal state and a well dispersed hexagonal state at moderate temperatures, and a sintered orthorhombic state at high temperatures ($\leq$ 400–500°C). It is possible to produce the well dispersed hexagonal phase from the sintered orthorhombic phase with an ammonia impregnation, which forms the ammonium rich precursor phases, and subsequent calcination at 300°C. The apparent increase in dispersion of the hexagonal phase may arise from some role of ammonia which results in a stronger MoO_3–SiO_2 interaction.

ACKNOWLEDGMENTS

Support from the Amoco Corporation and the Illinois Department of Commerce and Community Affairs (DCCA) is gratefully acknowledged. The authors are indebted to Dr. Joe Shyu of the Amoco Research Center in Naperville, Illinois for his collaboration with the XPS work, and to Professor Israel Wachs of Lehigh University for several stimulating discussions during the writing of the manuscript.

REFERENCES

1. Wang, L., and Hall, W. K., *J. Catal.* **77,** 232 (1982).
2. Gil-Llambias, F. J., Escudey-Castro, A. M.,

Lopez Agudo, A., and Garcia-Fierro, J. L., *J. Catal.* **90,** 323 (1984).
3. Leyer, J., Vielhaber, B., Zaki, M. I., Shuxian, Z., Weitkamp, J., and Knozinger, H., *Mater. Chem. Phys.* **13,** 301 (1985).
4. Vordonis, L., Koutsoukos, P. G., and Lycourghiotis, A., *J. Catal.* **98,** 296 (1986).
5. Margraf, R., Leyrer J., Taglauer, E., and Knozinger, H., *React. Kinet. Catal.* **35,** 261 (1987).
6. Okamoto, Y., and Imanaka, T., *J. Phys. Chem.* **92,** 7102 (1988).
7. Caceres, C. V., Fierro, J. L. G., Lazaro, J., Lopez Agudo, A., and Soria, J., *J. Catal.* **122,** 113 (1990).
8. Mulcahy, F. M., Fay, M. J., Proctor, A., Houalla, M., and Hercules, D. M., *J. Catal.* **124,** 231 (1990).
9. Spanos, N., Vordonis, L., Koutsoukos, P. G., and Lycourghiotis, A., *J. Catal.* **124,** 301 (1990).
10. Xie, Y., Gui, L., Liu, Y., Zhang, Y., Zhao, B., Yang, N., Guo, Q., Duan, L., Huan, H., Cai, X., and Tang, Y., in "Adsorption and Catalysis on Oxide Surfaces, eds. (M. Che and G. C. Bond, Eds.), p. 139. Elsevier, Amsterdam, 1985.
11. Leyer, J., Zaki, M. I., and Knozinger, H., *J. Phys. Chem.* **90,** 4775 (1986).
12. Margraf, R., Leyrer J., Knozinger, H., and Taglauer, E., *Surf. Sci.* **189/190,** 842 (1987).
13. Stampfl, S. R., Chen, Y., Dumesic, J. A., Niu, C., and Hill Jr., C. G., *J. Catal.* **105,** 445 (1987).
14. Haber, J., Machez, T., and Grabowski, R., *Solid State Ionics* **32/33,** 887 (1989).
15. Leyer, J., Mey, D., and Knozinger, H., *Surf. Sci.* **201,** 603 (1990).
16. Leyer, J., Mey, D., and Knozinger, H., *J. Catal.* **124,** 349 (1990).
17. Machej, T., Haber, J., Turek, A. M., and Wachs, I. E., *J. Appl. Catal.*, in press.
18. Cheng, C. P., and Schrader, G. L., *J. Catal.* **60,** 276 (1979).
19. Chan, S. S., Wachs, I. E., Murrell, L. L., Wang, L., and Hall, W. K., *J. Phys. Chem.* **88,** 5831 (1984).
20. Stencel, J. M., Makovsky, Sarkus, T. A., de Vries, J., Thomas, R., and Moulijn, J. A., *J. Catal.* **90,** 314 (1984).
21. Marcinkowska, K., Rodrigo, L., and Kaliaguine, S., *J. Mol. Catal.* **33,** 189 (1985).
22. Stencel, J. M., Diehl, J. R., D'Este, J. R., Makovsky, L. E., Rodrigo, L., Marcinkowska, K., Adnot, A., Roberge, P. C., and Kaliaguine, S., *J. Phys. Chem.* **90,** 4739 (1986).
23. Seyedmonir, S. R., and Howe, R. F., *J. Catal.* **110,** 216 (1988).
24. Marcinkowska, K., Rodrigo, L., Kaliaguine, S., and Roberge, P. C., *J. Catal.* **97,** 75 (1986).
25. Yermakov, Y. I., *Catal. Rev. Sci. Eng.* **13,** 77 (1976).
26. Iwasawa, Y., *Adv. Catal.* **35,** 265 (1987).
27. Candlin, J. P., and Thomas, H., *Adv. Chem. Ser.* **132,** 212 (1974).
28. Alsdorf, E., Hanke, W., Schnabel, K.-H., and Schreier, E., *J. Catal.* **98,** 82 (1986).
29. Bond, G. C., Flamerz, S., and van Mijk, L., *Catal. Today* **1,** 2286 (1987).
30. Fricke, R., Hanke, W., and Ohlman, G., *J. Catal.* **79,** 1 (1983).
31. Louis, C. Tatibouet, J. M., and Che, M., *J. Catal.* **109,** 354 (1988).
32. Yamagata, N., Owada, Y., Okazaki, S., and Tanabe, K., *J. Catal.* **47,** 358 (1977).
33. Wachs, I. E., *Chem. Eng. Sci.* **45,** 2561 (1990).
34. Deo, G., and Wachs, I. E., *J. Phys. Chem.*, in press.
35. Williams, C. G., Ekerdt, J. G., Jeng, Jih-Mirn, Hardcastle, F. D., and Wachs, I. E., *J. Phys. Chem.*, in press.
36. Williams, C. G., Ekerdt, J. G., Jeng, Jih-Mirn, Hardcastle, F. D., and Wachs, I. E., *J. Phys. Chem.*, in press.
37. Giordano N, Bart, J. C. J., Vaghi, A., Castellan, A., and Martinotti, G., *J. Catal.* **36,** 81 (1975).
38. de Beer, V. H. J., van der Aalst, M. J. M., Machiels, C. J., and Schuit, G. C. A., *J. Catal.* **43,** 78 (1976).
39. Zingg, D. S., Makovsky, L. E. Tischer, R. E., Brown, F. R., and Hercules, D. M., *J. Phys. Chem.* **84,** 2898 (1980).
40. Thomas, R., van Oers, E. M., de Beer, V. H. J., Medema, J., and Moulijn, J. A., *J. Catal.* **76,** 241 (1982).
41. Castellan, A., Bart, J. C. J., Vaghi, A., and Giordano, N., *J. Catal.* **42,** 162 (1976).
42. Prauliad, H., *J. Less-Common Metals* **54,** 387 (1977).
43. Gajardo, P., Pirotte, D., Grange, P., and Delmon, B., *J. Phys. Chem.* **83,** 1780 (1979).
44. Jeziorowski, H., Knozinger, H., Grange, P., and Gajardo, P., *J. Phys. Chem.* **84,** 1825 (1980).
45. Okamoto, Y., Imanaka, T., and Teranishi, S., *J. Phys. Chem.* **85,** 3798 (1981).
46. Marcinkowska, K., Kaliaguine, S., and Roberge, P. C., *J. Catal.* **90,** 49 (1984).
47. Rodrigo, L., Marcinkowska, K., Adnot, A., Roberge, P. C., Kaliaguine, S., Stencel, J. M., Makovsky, L. E., and Diehl, J. R., *J. Phys. Chem.* **90,** 2690 (1986).
48. Ono, T., Anpo, M., and Kubokawa, Y., *J. Phys. Chem.* **90,** 4780 (1986).
49. Kakuta, N., Tohji, K., and Udagawa, Y., *J. Phys. Chem.* **92,** 2583 (1988).
50. Fraser, W. A., Florio, J. V., Delgass, W. N., Robertson, W. S., *Surf. Sci.* **36,** 661 (1973).
51. Thomas, R., van Oers, E. M., de Beer, and Moulijn, J. A., *J. Catal.* **84,** 275 (1983).
52. Reddy, B. M., Rao, K. S. P., and Mastikhin, V. M., *J. Catal.* **113,** 556 (1988).
53. Pratt, K. C., Sanders, J. V., and Christov, V., *J. Catal.* **124,** 416 (1990).

54. Caiger, N. A., Crouch-Baker, S., Dickens, P. G., and James, G. S., *J. Solid State Chem.* **67,** 369 (1987).
55. Olenkova, I. P., Tarasova, D. V., Kustova, G. N., Aleshina, G. I., and Mikhailenko, E. L., *React. Kinet. Catal. Lett.* **9,** 221 (1978).
56. Sotani, N., *Bull. Chem. Soc. Jpn.* **48,** 1820 (1975).
57. Datta, A., Regalbuto, J. R., and Allen, C. W., *Ultramicroscopy* **29,** 233 (1989).
58. Louis, C., Tatibouet, J. M., and Che, M., *J. Catal.* **109,** 354 (1988).
59. JCPD file number 37-379.
60. Hayden, T. F., and Dumesic, J. A., *J. Catal.* **103,** 366 (1987).
61. Grove, C. L., and Schmidt, L. D., *Appl. Surf. Sci.* **35,** 199 (1988–1989).
62. Parks, C. A., *Chem. Rev.* **65,** 177 (1965).
63. Noh, J. S., and Schwarz, J. A., *J. Colloid Interface Sci.* **130,** 157 (1989).
64. Wang, L., and Hall, W. K., *J. Catal.* **66,** 251 (1980).
65. Jeziorowski, H., and Knozinger, H., *J. Phys. Chem.* **83,** 1166 (1979).
66. Okamoto, Y., Tomioka, H., Katoh, Y., Imanaka, T., and Teranishi, S., *J. Phys. Chem.* **84,** 1833 (1980).
67. Sotani, N., Masuda, S., Iwata, Y., and Hasegawa, M., *in* "Proceedings, 3rd International Conference on Chemical Uses of Molybdenum, 1979," p. 157.
68. Dufaux, M., Che, M., and Nacchache, C., *J. Chem. Phys.* **67,** 527 (1970).
69. Iler, R. K., "The Chemistry of Silica," John Wiley & Sons, New York, 1979.
70. Iwasawa, Y., *in* "Tailored Metal Catalysts" (Y. Irv, Ed.), p. 1. D. Reidel, Boston, 1986.
71. Peri, J. B., Hensley, A. L., Jr., *J. Phys. Chem.* **72,** 2926 (1968).
72. Haber, J., *Pure Appl. Chem.* **56,** 1663 (1984).
73. Ruckenstein, E., and Lee, S. H., *J. Catal.* **104,** 259 (1987).